ELSEVIER

www.elsevier.nl/locate/jorganchem

Journal of Organometallic Chemistry 605 (2000) 184–192

Journal of Organometallic Chemistry

Organometallic complexes for nonlinear optics[☆]
Part 20. Syntheses and molecular quadratic hyperpolarizabilities of alkynyl complexes derived from (*E*)-4,4′-$HC{\equiv}CC_6H_4N{=}NC_6H_4NO_2$

Andrew M. McDonagh[a], Nigel T. Lucas[a], Marie P. Cifuentes[a],
Mark G. Humphrey[a,*], Stephan Houbrechts[b], André Persoons[b]

[a] *Department of Chemistry, Australian National University, Canberra, ACT 0200, Australia*
[b] *Laboratory for Chemical and Biological Dynamics, University of Leuven, Celestijnenlaan 200D, B-3001 Leuven, Belgium*

Received 18 April 2000; accepted 18 May 2000

Abstract

The syntheses of the alkyne (*E*)-4,4′-$HC{\equiv}CC_6H_4N{=}NC_6H_4NO_2$ (**1**) and alkynyl complexes $L_nM\{(E)\text{-}4,4'\text{-}C{\equiv}CC_6H_4N{=}NC_6H_4NO_2\}$ [L_nM = *trans*-$[RuCl(dppm)_2]$ (**2**), $Ru(PPh_3)_2(\eta\text{-}C_5H_5)$ (**3**), $Au(PPh_3)$ (**4**)] are reported. A structural study of **2** reveals *E* stereochemistry about the azo-linkage. Electrochemical data for the ruthenium complexes reveal that the azo-linkage in complexes **2** and **3** perturbs the metal-centred oxidation potential compared to all other alkynyl complexes of similar composition. Quadratic optical nonlinearities by hyper-Rayleigh scattering (HRS) at 1064 nm are very large for **2** and **3**, but resonance-enhanced. Comparison of HRS data for **4** with those of $Au\{(E)\text{-}4,4'\text{-}C{\equiv}CC_6H_4X{=}CHC_6H_4NO_2\}(PPh_3)$ (X = CH, N) reveals that complex **4** has a significantly larger quadratic nonlinearity than its ene- or imino-linked analogues. © 2000 Elsevier Science S.A. All rights reserved.

Keywords: Ruthenium; Gold; Cyclic voltammetry; X-ray structure; Quadratic hyperpolarizabilities; Alkynyl; Nonlinear optics

1. Introduction

Organic compounds with a donor-π-bridge-acceptor composition can have significant nonlinear optical (NLO) properties, and have a potential for use in a variety of technologically important processes [1]. For this reason, studies have been promulgated to uncover molecular structure–NLO activity relationships. One molecular modification, which has significant impact on quadratic NLO merit, is the variation of the length and composition of the π-system. In particular, extending a π-system by incorporating arylethenyl groups into the bridge is an efficient way to increase the quadratic NLO coefficient [2–7].

One possible change to this efficient molecular composition is to modify the ethenyl linkages by introduction of heteroatoms. Replacing the *trans*-CH=CH linkage in 4-*N*,*N*-dimethylamino-4′-nitrostilbene by a *trans*-N=CH group, to afford the corresponding benzylideneaniline, results in a 25% decrease in both experimentally-obtained [by EFISH (electric field-induced second harmonic generation) at 1.36 μm] molecular quadratic nonlinearity β and two-level-corrected nonlinearity β_0 [8]. While the current work was in progress, this system was reinvestigated, together with the imino-linked and azo-linked analogues which result from replacing the *trans*-CH=CH linkage by a *trans*-CH = N group or *trans*-N=N group, respectively [9]. β_0 data (EFISH at 1.91 μm) revealed that the first hyperpolarizabilities of *trans*-CH=CH and N=N bridged donor–acceptor compounds are of comparable magnitude, but that substitution of one carbon by a nitrogen atom (in proceeding from ene-linked to imino-linked compound) results in a significant reduction of second-order NLO activity, confirming the findings of the earlier study.

[☆] Part 19: A.M. McDonagh, M.P. Cifuentes, N.T. Lucas, M.G. Humphrey, S. Houbrechts, A. Persoons, J. Organomet. Chem. (in press).

* Corresponding author. Tel.: +61-2-62492927; fax: +61-2-62490760.

E-mail address: mark.humphrey@anu.edu.au (M.G. Humphrey).

PII: S0022-328X(00)00311-9

Very recently, zinc complexes bearing 4,4′-bis(dialkylaminophenylazo)-2,2′-bipyridine, 4,4′-bis(dialkylaminophenylimino)-2,2′-bipyridine and 4,4′-bis(dialkylaminophenylalkenyl)-2,2-bipyridine ligands have been examined by EFISH [10]. A small increase in nonlinearity was observed on replacing CH by N, but this was largely ascribed to resonance enhancement.

Organometallics can also be prepared with a donor–π-bridge-acceptor composition, but have additional design flexibility compared to organics. The metal, co-ligands, coordination geometry and oxidation state can all be varied, which may impact favourably on NLO merit. Not surprisingly, the quadratic and cubic NLO properties of organometallic complexes have come under intense scrutiny [11–15]. We have shown previously that alkynyl complexes with a ligated metal as donor group are amongst the most efficient organometallics for their quadratic NLO response [16–22], with nonlinearities comparable in magnitude to the best organics. Similar to the above studies with alkenes and imines, we have shown (by HRS at 1.06 μm) that complexes $L_nM\{(E)\text{-}4,4'\text{-}C{\equiv}CC_6H_4CH{=}CHC_6H_4NO_2\}$ $\{L_n = Ru(PPh_3)_2(\eta\text{-}C_5H_5)$, $Au(PPh_3)$, $Ni(PPh_3)(\eta\text{-}C_5H_5)\}$ are significantly more efficient than $L_nM\{(E)\text{-}4,4'\text{-}C{\equiv}CC_6H_4N{=}CHC_6H_4NO_2\}$. Computational studies utilizing ZINDO confirmed these observations, but also suggested that the azo-linked analogue should be twice as efficient as the ene-linked example [16]. However, no complexes with this alkynyl ligand were prepared, as the corresponding alkyne (E)-4,4′-$HC{\equiv}CC_6H_4N{=}NC_6H_4NO_2$ was unknown. We now report the synthesis of this alkyne and some alkynyl metal derivatives, a structural study of a representative complex, electrochemical and quadratic NLO data for these new compounds, and comparison with previously reported data for the cognate ene- and imino-linked analogues.

2. Results and discussion

2.1. Synthesis and characterization of (*E*)-4,4′-$HC{\equiv}CC_6H_4N{=}NC_6H_4NO_2$ (*1*)

The preparation of (E)-4,4′-$HC{\equiv}CC_6H_4N{=}NC_6H_4NO_2$ (**1**) is outlined in Scheme 1; diazotization of commercially available (E)-4,4′-$H_2NC{\equiv}CC_6H_4N{=}NC_6H_4NO_2$ followed by reaction with iodide [23] affords the aryl iodide (E)-4,4′-$IC_6H_4N{=}NC_6H_4NO_2$ (37%) which is then reacted in the standard manner [24] to give the terminal alkyne **1** (45%). Isolation of the trimethylsilyl-protected alkyne intermediate offered no advantage in terms of yield or purity.

The UV–vis spectra of (E)-4,4′-$IC_6H_4N{=}NC_6H_4NO_2$ and **1** contain absorption bands at 28 300 and 28 400 cm^{-1}, respectively, assigned to a $\pi \rightarrow \pi^*$ transition, and much weaker bands at 21 400 and at 21 700 cm^{-1}, respectively, assigned to a $n \rightarrow \pi^*$ transition. Characteristic symmetric and asymmetric N=O stretches are observed in the IR spectrum of (E)-4,4′-$IC_6H_4N{=}NC_6H_4NO_2$ at 1347 and 1527 cm^{-1}, respectively, and in the IR spectrum of **1** at 1346 and 1527 cm^{-1}, respectively. The ^{1}H-NMR spectrum of **1** contains a signal at 3.27 ppm assigned to the proton of the terminal alkyne.

2.2. Synthesis and characterization of $L_nM\{(E)\text{-}4,4'\text{-}C{\equiv}CC_6H_4N{=}NC_6H_4NO_2\}$ [L_nM = *trans*-RuCl(dppm)$_2$ (*2*), Ru(PPh$_3$)$_2$(η-C$_5$H$_5$) (*3*), Au(PPh$_3$) (*4*)]

The preparation of the new alkynyl complexes **2** [25], **3** [26], and **4** [17] followed published procedures for the preparation of phenyl- or 4-nitrophenyl-alkynyl analogues, and are shown in Schemes 2–4. Reaction of *cis*-[RuCl$_2$(dppm)$_2$], sodium hexafluorophosphate and the terminal alkyne in dichloromethane at room temperature (r.t.) afforded *trans*-[Ru{(E)-4,4′-C=CHC$_6$-

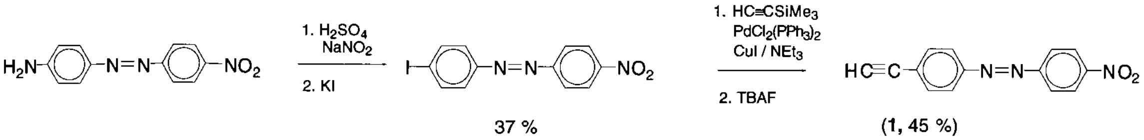

Scheme 1. Preparation of (E)-4,4′-$HC{\equiv}CC_6H_4N{=}NC_6H_4NO_2$ (**1**).

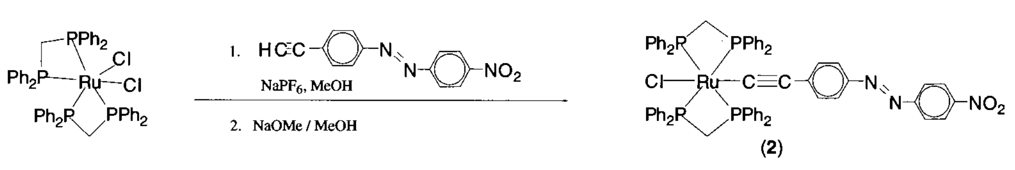

Scheme 2. Preparation of *trans*-[Ru{(E)-4,4′-$C{\equiv}CC_6H_4N{=}NC_6H_4NO_2$}Cl(dppm)$_2$] (**2**).

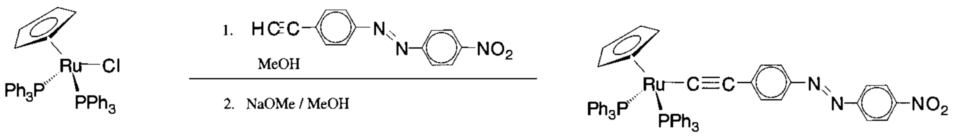

(3)

Scheme 3. Preparation of [Ru{(*E*)-4,4′-$C{\equiv}CC_6H_4N{=}NC_6H_4NO_2$}$(PPh_3)_2$(η-$C_5H_5$)] (**3**).

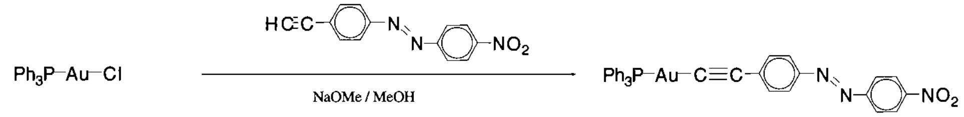

(4)

Scheme 4. Preparation of [Au{(*E*)-4,4′-$C{\equiv}CC_6H_4N{=}NC_6H_4NO_2$}($PPh_3$)] (**4**).

$H_4N{=}NC_6H_4NO_2$}Cl$(dppm)_2$]PF_6. Subsequent deprotonation with base in situ afforded the desired alkynyl complex **2** in good yield (62%). Reaction of [RuCl$(PPh_3)_2$(η-C_5H_5)] with terminal alkyne in refluxing methanol afforded the vinylidene complex [Ru{(*E*)-4,4′-$C{=}CHC_6H_4N{=}NC_6H_4NO_2$}$(PPh_3)_2$(η-$C_5H_5$)]$^+$ which, unlike its bis(dppm) analogue above, does not require the presence of large counterions (such as hexafluorophosphate) for stability, the displaced chloride presumably being sufficient. The vinylidene complex was deprotonated with base in situ to afford **3** in 51% yield. A mixture of (triphenylphosphine)gold chloride, (*E*)-4,4′-$HC{\equiv}CC_6H_4N{=}NC_6H_4NO_2$ and sodium methoxide solution was stirred in dichloromethane for 18 h to give [Au{(*E*)-4,4′-$C{\equiv}CC_6H_4N{=}NC_6H_4NO_2$}($PPh_3$)] (**4**) in 71% yield.

The new alkynyl complexes were characterized by FABMS, satisfactory microanalyses, UV–vis and IR spectroscopy, ^{1}H-, ^{31}P- and ^{13}C-NMR spectroscopy. The FAB mass spectrum of **2** and **3** contain molecular ions, with fragmentation of the former proceeding by loss of chloro and alkynyl ligands to afford a peak corresponding to [Ru$(dppm)_2$]$^+$, and fragmentation of the latter proceeding by successive loss of alkynyl and phosphine ligand to afford a peak corresponding to [Ru(PPh_3)(η-C_5H_5)]$^+$. The FAB mass spectrum of **4** does not contain a molecular ion, but rather signals corresponding to [Au$(PPh_3)_x$]$^+$ ($x = 1, 2$). The IR spectra contain characteristic bands assigned to ν(C≡C) at 2061 (**2**), 2054 (**3**) and 2113 (**4**) cm^{-1}. The ^{31}P-NMR spectra contain singlet resonances at −6.3 (**2**), 50.7 (**3**) and 42.6 (**4**) ppm, with that of the first-mentioned confirming the *trans* stereochemistry of the chloro and alkynyl ligands.

2.3. X-ray structural study of trans-[Ru{(E)-4,4′-$C{\equiv}CC_6H_4N{=}NC_6H_4NO_2$}Cl$(dppm)_2$] (2)

The identity of **2** was confirmed by a single-crystal X-ray diffraction study. Selected bond lengths and angles are listed in Table 1, and an ORTEP diagram showing the molecular structure and atomic labeling scheme is displayed in Fig. 1.

The structural study confirms the octahedral geometry at ruthenium and the *trans*-disposed chloride and alkynyl ligands, and reveals the *E* stereochemistry about the azo-linkage. Bond distances and angles involving the diphosphine ligands are unexceptional. Important bond lengths about the metal center are similar to those of the related donor-bridge-acceptor complexes *trans*-[Ru(4-$C{\equiv}CC_6H_4NO_2$)Cl$(dppm)_2$] (**5**) [37] and *trans*-[Ru(4,4′-$C{\equiv}CC_6H_4C_6H_4NO_2$)Cl$(dppm)_2$] (**6**) [27] (Table 1). We have shown previously by semi-empirical

Table 1
Selected bond lengths (Å) and angles (°) for *trans*-[Ru{(*E*)-4,4′-$C{\equiv}CC_6H_4N{=}NC_6H_4NO_2$}Cl$(dppm)_2$] (**2**), *trans*-[Ru(4-$C{\equiv}CC_6H_4$-NO_2)Cl$(dppm)_2$] (**5**) and *trans*-[Ru(4,4′-$C{\equiv}CC_6H_4C_6H_4NO_2$)-Cl$(dppm)_2$] (**6**)

	4	**5**	**6**
Bond lengths			
Ru–Cl	2.508(2)	2.483(2)	2.499(1)
Ru–P(1)	2.322(2)	2.332(2)	2.330(1)
Ru–P(2)	2.352(2)	2.332(2)	2.358(1)
Ru–P(3)	2.349(2)	2.358(2)	2.350(1)
Ru–P(4)	2.355(2)	2.379(2)	2.361(1)
Ru–C(1)	1.974(7)	1.998(7)	1.994(4)
C(1)–C(2)	1.224(9)	1.190(8)	1.198(6)
C(2)–C(3)	1.406(9)	1.428(8)	1.439(7)
N(1)–N(2)	1.263(9)		
C(12)–N(3)	1.47(1)	1.467(9)	1.481(6)
N(3)–O(1)	1.22(1)	1.220(8)	1.237(7)
N(3)–O(2)	1.18(1)	1.207(8)	1.226(7)
Bond angles			
P(1)–Ru–P(2)	72.20(7)	70.98(6)	71.85(5)
P(3)–Ru–P(4)	71.47(7)	70.18(6)	71.63(5)
Cl–Ru–C(1)	173.1(2)	177.7(2)	175.2(1)
Ru–C(1)–C(2)	175.2(6)	176.8(5)	177.9(4)
C(1)–C(2)–C(3)	179.8(9)	168.4(7)	179.1(5)
C(6)–N(1)–N(2)	112.9(8)		
N(1)–N(2)–C(9)	111.5(8)		
O(1)–N(3)–O(2)	124(1)		

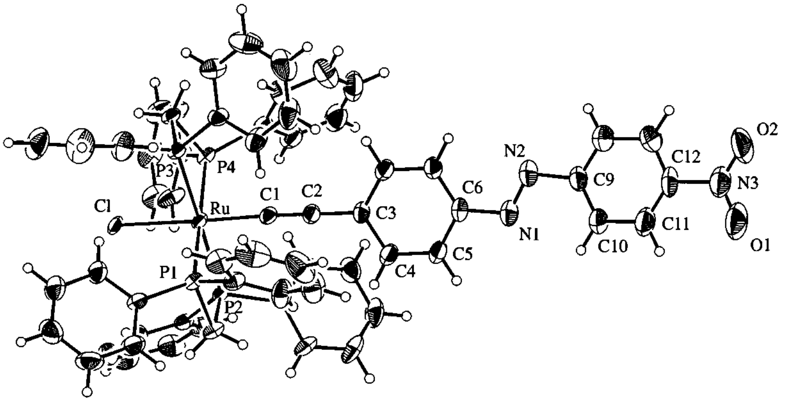

Fig. 1. Molecular geometry and atomic labelling scheme for *trans*-[Ru{(*E*)-4,4′-C≡CC$_6$H$_4$N=NC$_6$H$_4$NO$_2$}Cl(dppm)$_2$] (**2**). Non-hydrogen atoms are depicted with 30% thermal ellipsoids; hydrogen atoms are placed in calculated positions with arbitrary bond lengths of 0.95 Å.

ZINDO that short Ru–C distances lead to large quadratic nonlinearities [28]; significantly, the Ru–C(1) distances in these complexes are amongst the shortest for alkynyl–ruthenium complexes. The Cl–Ru–C(1) and Ru–C(1)–C(2) angles deviate slightly from the idealized 180°, presumably a result of packing effects. Lack of co-planarity in adjacent phenyl rings may lead to a diminution in quadratic NLO merit from that expected for a co-planar disposition; we have previously reported that the rotation from co-planarity of adjacent phenyl groups in **6** reduces computationally-derived molecular NLO activity [27]. For **2**, the two phenylene units of the acetylide ligand are not co-planar, with the angle between the two planes being 16.9°. The centrosymmetric space group suggests that no bulk NLO response would be observed; the molecules have packed pair-wise with dipoles aligned antiparallel.

2.4. Electrochemical studies

In order to gain insight into the electronic environment of the metal atom in the new alkynyl complexes, the redox properties of **2** and **3** were examined by cyclic voltammetry; the results are summarized in Table 2, together with data for some related complexes for comparison.

Cyclic voltammetric scans of complexes **2** and **3** using potentials of 0–1.0 V each show an electrochemically reversible wave with similar potentials (0.62 for **2**, 0.66 V for **3**), attributed to the metal-centered Ru$^{II/III}$ oxidation process. We have previously reported that progressing from the 4-nitrophenyl–alkynyl complexes *trans*-[Ru(4-C≡CC$_6$H$_4$NO$_2$)Cl(dppm)$_2$] (**5**) and Ru(4-C≡CC$_6$H$_4$NO$_2$)(PPh$_3$)$_2$(η-C$_5$H$_5$) (**7**) to *trans*-[Ru{(*E*)-4,4′-C≡CC$_6$H$_4$CH=CHC$_6$H$_4$NO$_2$}Cl(dppm)$_2$] (**8**) and Ru{(*E*)-4,4′-C≡CC$_6$H$_4$CH=CHC$_6$H$_4$NO$_2$}(PPh$_3$)$_2$(η-C$_5$H$_5$) (**9**) leads to a decrease of 0.16–0.18 V in oxidation potential [18,22]. More subtle variations (changing the bridging unit in the extended chain acetylide complexes across the series 4,4′-C≡C$_6$H$_4$C$_6$H$_4$NO$_2$, 4,4′-C≡CC$_6$H$_4$C≡C$_6$H$_4$NO$_2$, (*E*)-4,4-C≡C$_6$H$_4$N=CHC$_6$H$_4$-NO$_2$, (*E*)-4,4′-C≡CC$_6$H$_4$CH=CHC$_6$H$_4$NO$_2$) did not affect the Ru$^{II/III}$ couple significantly [18]. Extending the comparison to the new azo-linked complexes reveals that oxidation potentials increase as E^0: **8**, **9** (extended chain nitrophenylalkynyl complexes) < **2**, **3** (azo-linked complexes) < **5**, **7** (4-nitrophenyl–alkynyl complexes); thus, the azo-linkage produces a perturbation of the oxidation potential of the Ru$^{II/III}$ couple compared to other extended chain acetylides. Anodic scans to −1.6 V show that, in contrast to the single nitro-centred reduction observed in cyclic voltammograms of the nitroaryl–alkynyl–ruthenium complexes, the azo-linked **2** and **3** each have two reduction waves, the second process presumably due to a reduction process involving the azo-linkage.

2.5. Nonlinear optical studies

Quadratic optical nonlinearities of the new compounds were determined using the hyper-Rayleigh scattering (HRS) technique at 1064 nm. The results of these studies are given in Table 2, together with linear optical absorption data, two-level-corrected quadratic nonlinearities, results for related ruthenium and gold complexes, and data for the relevant alkynes for comparison. We have previously noted that quadratic nonlinearities for gold and ruthenium–alkynyl complexes are larger than those for the parent organic alkynes [30]. A similar result is observed with the new compounds; progression from **1** to **2**–**4** leads to significant increases in both observed and two-level corrected nonlinearities. Data for the new alkynyl complexes **2**–**4** are much larger than those for the phenylalkynyl (**10**–**12**) or nitrophenylalkynyl (**5**, **7**, **13**) analogues. This may not be surprising given that proceeding from **10**–**12** to complexes **2**–**4** involves the introduction of an acceptor substituent and proceeding from **5**, **7**, **13** to

2–**4** involves chromophore chain-lengthening, i.e. two structural modifications which are known to enhance quadratic NLO merit. Comparison of the azo-linked complexes **2**–**4** with the ene-linked (**8**, **9**, **14**) and imino-linked (**15**, **16**) analogues reveals that the nonlinearity increases on proceeding from the imino-linked complexes to the ene-linked and azo-linked complex analogues. Comparison between ene-linked and azo-linked ruthenium complexes is difficult given the proximity of the linear optical absorption maxima to the second-harmonic wavelength (532 nm); resonance enhancement and damping render such comparisons very difficult. In contrast, the gold-containing complexes **4**, **14** and **16** have absorption maxima far removed from the second harmonic, permitting comment on the effect of bridging unit variation. Data for both experimentally obtained and two-level-corrected nonlinearities follow the trend: imino-linked (**16**) < ene-linked (**14**) < azo-linked (**4**) complex.

3. Conclusions

Synthetic routes into the terminal alkyne (*E*)-4,4′-$HC\equiv CC_6H_4N{=}NC_6H_4NO_2$ and derivative metal alkynyl complexes have been developed. An X-ray structural study of *trans*-[Ru{(*E*)-4,4′-$C\equiv CC_6H_4N{=}NC_6H_4NO_2$}-Cl(dppm)$_2$] (**2**) confirms the *E* stereochemistry of the azo-linkage. Electrochemical data reveals that the metal-centered oxidation is sensitive to bridging atom variation. NLO measurements using the HRS technique show that the new ruthenium complexes bearing the

Table 2
Cyclic voltammetric data, experimental linear optical spectroscopic and quadratic nonlinear optical response parameters

Compound	$E^\circ_{\mathrm{RuII/III}}$ (V) [a]	$E^\circ_{\mathrm{A0/-1}}$ (V) [a]	λ_{max} (nm) [b]	β [b,c]	β_0 [d]	Reference
	[i_{pc}/i_{pa}]	[i_{pa}/i_{pc}]	[ε (10^4 M^{-1} cm^{-1})]	(10^{-30} esu)	(10^{-30} esu)	
(*E*)-4,4′-$HC\equiv CC_6H_4N{=}NC_6H_4NO_2$ (**1**)			381 (2.7)	59	29	This work
trans-[Ru{(*E*)-4,4′-$C\equiv CC_6H_4N{=}NC_6H_4NO_2$}-Cl(dppm)$_2$] (**2**)	0.62 (1.0)	−0.63 (1.0) −1.03 (0.5)	583 (2.7)	1649	232	This work
[Ru{(*E*)-4,4′-$C\equiv CC_6H_4N{=}NC_6H_4NO_2$}(PPh$_3$)$_2$-(η-C$_5H_5$)] (**3**)	0.66 (1.0)	−0.74 (1.0) −0.97 (0.5)	565 (2.9)	1627	149	This work
[Au{(*E*)-4,4′-$C\equiv CC_6H_4N{=}NC_6H_4NO_2$}(PPh$_3$)] (**4**)			398 (3.3)	180	68	This work
(*E*)-4,4′-$HC\equiv CC_6H_4CH{=}CHC_6H_4NO_2$			358 (3.3)	55	27	[17]
trans-[Ru{(*E*)-4,4′-$C\equiv CC_6H_4CH{=}CHC_6H_4NO_2$}-Cl(dppm)$_2$] (**8**)	0.56 (1.0)	−0.87 (0.4)	490 (2.6)	1964	235	[22]
[Ru{(*E*)-4,4′-$C\equiv CC_6H_4CH{=}CHC_6H_4NO_2$}(PPh$_3$)$_2$-(η-C$_5H_5$)] (**9**)	0.55 (0.9)	−0.92 (0.3)	476 (2.6)	1455	232	[16,18,29]
[Au{(*E*)-4,4′-$C\equiv CC_6H_4CH{=}CHC_6H_4NO_2$}(PPh$_3$)] (**14**)			386 (3.8)	120	49	[17]
4-$HC\equiv CC_6H_4NO_2$			288 (1.5)	14	9	[17]
trans-[Ru(4-$C\equiv CC_6H_4NO_2$)Cl(dppm)$_2$] (**5**)	0.72 (0.9)	−1.08 (0.7)	473 (1.8)	767	129	[22]
[Ru(4-$C\equiv CC_6H_4NO_2$)(PPh$_3$)$_2$(η-C$_5$H$_5$)] (**7**)	0.73 (1.0)	−1.08 (1.0)	460 (1.1)	468	96	[16,18,29]
[Au(4-$C\equiv CC_6H_4NO_2$)(PPh$_3$)] (**13**)			338 (2.5)	22	12	[17]
(*E*)-4,4′-$HC\equiv CC_6H_4N{=}CHC_6H_4NO_2$			355 (1.4)	36	18	[16,18,29]
[Ru{(*E*)-4,4′-$C\equiv CC_6H_4N{=}CHC_6H_4NO_2$}(PPh$_3$)$_2$-(η-C$_5H_5$)] (**15**)	0.57 (1.0)	−0.79 (0.5)	496 (1.3)	840	86	[16]
[Au{(*E*)-4,4′-$C\equiv CC_6H_4N{=}CHC_6H_4NO_2$}(PPh$_3$)] (**16**)			392 (2.1)	85	34	[17]
trans-[Ru($C\equiv CPh$)Cl(dppm)$_2$] (**10**)	0.55 (1.0)		308 (1.7)	20	12	[22]
[Ru(4-$C\equiv CPh$)(PPh$_3$)$_2$(η-C$_5$H$_5$)] (**11**)	0.55 (0.7)		310 (2.0)	16	10	[18]
[Au($C\equiv CPh$)](PPh$_3$) (**12**)			296 (1.3)	6	4	[17]

[a] Ag/AgCl reference; CH_2Cl_2 solvent.

[b] THF solvent.

[c] All compounds are optically transparent at the fundamental frequency. HRS at 1064 nm; values ± 10%, using *p*-nitroaniline ($\beta = 21.4 \times 10^{-30}$ esu) as a reference.

[d] Data corrected for resonance enhancement at 532 nm using the two-level model with $\beta_0 = \beta[1-(2\lambda_{max}/1064)^2][1-(\lambda_{max}/1064)^2]$; damping factors are not included.

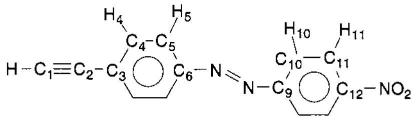

Fig. 2. NMR numbering scheme.

azo-linked alkynyl ligand have very large second-order molecular nonlinearities. The gold complex **4** is optically transparent at both the fundamental and second-harmonic wavelengths, permitting a comparison of the effect of ligand variation to be made. Complex **4** has significantly larger quadratic nonlinearity than its ene-linked or imino-linked analogues.

We have recently investigated another possibility for enhancing quadratic NLO merit by modification of the alkynyl ligand, namely utilizing indoanilinoalkynyl ligands [1]. Replacing the indoanilinoalkynyl ligand $C{\equiv}C\text{-}4\text{-}C_6H_4N{=}\overline{CCH{=}C^{t}BuC(O)C^{t}Bu{=}CH}$ by the azo-linked alkynyl ligand results in a dramatic increase in quadratic nonlinearity for both the chlorobis(dppm)ruthenium system (417×10^{-30} esu cf 1649×10^{-30} esu) and (cyclopentadienyl)bis(triphenylphosphine)ruthenium system (658×10^{-30} esu cf 1627×10^{-30} esu). Significantly, the optical absorption maxima are two to three times more intense for the azo-linked complexes **2** and **3** in the present study than their indoanilino–alkynyl complex analogues. Modification of the arylalkynyl ligand by incorporation of an azo bridging unit is an effective way to enhance nonlinearity. Oligomeric and polymeric compounds for nonlinear optics are frequently constructed using yne- or ene-linkages; the current studies suggest that attention should also be focussed on azo-linkages for constructing efficient NLO materials.

4. Experimental

4.1. General conditions, reagents and instruments

All reactions were performed under a nitrogen atmosphere with the use of Schlenk techniques unless otherwise stated. Dichloromethane was dried by distilling over CaH_2, methanol was dried by distilling over Mg–I_2, and tetrahydrofuran was dried by distilling over sodium–benzophenone; other solvents were used as received. 'Pet. spirit' refers to a fraction of petroleum ether of boiling range 60–80°C. Chromatography was on silica gel (230–400 mesh ASTM) or ungraded basic alumina.

The following were prepared by literature procedures: $[RuCl(PPh_3)_2(\eta\text{-}C_5H_5)]$ [31], *cis*-$[RuCl_2(dppm)_2]$ [38], $[AuCl(PPh_3)]$ [32]. Sodium methoxide solutions were prepared by reacting sodium with dry methanol. Dichlorobis(triphenylphosphine)palladium(II) was prepared by stirring two equivalents of triphenylphosphine with palladium(II) chloride in dimethylformamide at reflux for 2 h. The resulting precipitate was collected and recrystallized from chloroform. Sodium hexafluorophosphate (Aldrich) was recrystallized from acetonitrile before use. Trimethylsilylethyne (Aldrich), copper(I) iodide (Unilab), tetra-*n*-butylammonium fluoride (1 M solution in tetrahydrofuran) (Aldrich), sulfuric acid (98%) (Univar), (*E*)-4,4′-$H_2NC_6H_4N{=}NC_6H_4NO_2$ (Disperse Orange 3, 95%) (Aldrich), sodium nitrite (M & B), potassium iodide (M & B) and anhydrous magnesium sulfate (Aldrich) were used as received.

EI (electron impact) mass spectra [both unit resolution and high resolution (HR)] were recorded using a VG Autospec instrument (70 eV electron energy, 8 kV accelerating potential) and secondary ion mass spectra were recorded using a VG ZAB 2SEQ instrument (30 kV Cs^+ ions, current 1 mA, accelerating potential 8 kV, 3-nitrobenzyl alcohol matrix) at the Research School of Chemistry, Australian National University; peaks are reported as m/z (assignment, relative intensity). Microanalyses were carried out at the Research School of Chemistry, Australian National University. Infrared spectra were recorded as dichloromethane solutions using a Perkin–Elmer System 2000 FTIR. ^1H- (300 MHz), ^{13}C- (75 MHz) and ^{31}P- (121 MHz) NMR spectra were recorded using a Varian Gemini-300 FT NMR spectrometer and are referenced to residual solvent (^1H, ^{13}C) or external 85% H_3PO_4 (^{31}P). The assignments follow the numbering schemes shown in Fig. 2. UV-vis spectra were recorded using either a Cary 4 or Cary 5 spectrophotometer of solutions in THF in 1 cm cells. Electrochemical measurements were recorded using a MacLab 400 interface and MacLab potentiostat from ADInstruments. The supporting electrolyte was 0.1 M $[NBu^n_4][PF_6]$ in distilled, deoxygenated CH_2Cl_2. Solutions containing ca. 1×10^{-3} M complex were maintained under nitrogen. Measurements were carried out using Pt disc working-, Pt auxiliary- and Ag–AgCl reference-electrodes, such that the ferrocene–ferrocenium redox couple was located at 0.56 V. Scan rates were 100 mV s^{-1}.

4.2. Synthesis of (E)-4,4′-$HC{\equiv}CC_6H_4N{=}NC_6H_4NO_2$ (1)

4.2.1. (E)-4,4′-$IC_6H_4N{=}NC_6H_4NO_2$

No attempt to exclude air was made during this procedure. Concentrated sulfuric acid (2 ml) was added to water (250 ml) in a 500 ml round-bottomed flask. (*E*)-4,4-$H_2NC_6H_4N{=}NC_6H_4NO_2$ (2.0 g, 8.3 mmol) was added and the mixture stirred until a fine suspension was formed (ca. 10 min). Sodium nitrite (800 mg, 11.6 mmol) was added and the mixture stirred at r.t. for 1 h. The mixture was filtered through a plug of Celite and an aqueous solution of potassium iodide (2.5 g, 15 mmol in 50 ml of water) was added to the filtrate with stirring, whereupon a precipitate formed. The mixture was extracted with dichloromethane, the organic phase separated and dried with magnesium sulfate, and the solvent removed on a rotary evaporator. The residue was then purified by column chromatography on silica. Yield was 1.02 g (37%) of an orange–brown powder. HR MS (EI) $C_{12}H_8IN_3O_2$: Calc. 352.9661, Found 352.9665. UV–vis (λ_{max}, nm [ε, M^{-1} cm^{-1}]): 461 [1500], 353 [28 300]. IR (cm^{-1}): 1527 (m) ν_{as}(N=O), 1347 (w) ν_s(N=O). ^{1}H-NMR: δ 7.68 (d, $J_{HH} = 9$ Hz, 2H, H_4), 7.90 (d, $J_{HH} = 9$ Hz, 2H, H_5), 8.02 (d, $J_{HH} = 9$ Hz, 2H, H_{10}), 8.37 (d, $J_{HH} = 9$ Hz, 2H, H_{11}).

4.2.2. *(E)-4,4′-HC≡CC$_6$H$_4$N=NC$_6$H$_4$NO$_2$ (**1**)*

(*E*)-4,4′-$IC_6H_4N{=}NC_6H_4NO_2$ (250 mg, 0.71 mmol) and trimethylsilylethyne (0.4 ml, 2.8 mmol) were dissolved in tetrahydrofuran (5 ml) with stirring. Triethylamine (2 ml) was added followed by dichlorobis-(triphenylphosphine)palladium(II) (50 mg, 0.071 mmol) and copper(I) iodide (20 mg, 0.11 mmol), and the resultant mixture was stirred for 1 h. The mixture was then passed through a silica plug eluting with dichloromethane. The volume was reduced to ca. 40 ml on a rotary evaporator and a solution of tetra-*n*-butylammonium fluoride (1 ml, 1 M solution in tetrahydrofuran) was added without the exclusion of air. The mixture was stirred for 5 min and then the solvent was removed on a rotary evaporator. The residue was purified by column chromatography on silica eluting with 1:1 dichloromethane–pet. spirit. The yield was 89 mg (45%) of an orange powder. EI MS: 251 ([M]$^+$, 45), 150 ([$N_2C_6H_4NO_2$]$^+$, 5), 129 ([$HC{\equiv}CC_6H_4N_2$]$^+$, 35), 101 ([$HC{\equiv}CC_6H_4$]$^+$, 100). Anal. Calc. for $C_{14}H_9N_3O_2$: C, 66.93; H, 3.61; N, 16.73. Found: C, 66.03; H, 3.48; N, 16.04%. UV–vis (λ_{max}, nm [ε, M^{-1} cm^{-1}]): 461 [860], 352 [27 200]. IR (cm^{-1}): 1527 (m) ν_{as}(N=O), 1346 (m) ν_s(N=O). ^{1}H-NMR: δ 3.27 (s, 1H, HC≡C), 7.65 (d, 2H, $J_{HH} = 9$ Hz, H_4), 7.92 (d, 2H, $J_{HH} = 9$ Hz, H_5), 8.02 (d, 2H, $J_{HH} = 9$ Hz, H_{10}), 8.38 (d, 2H, $J_{HH} = 9$ Hz, H_{11}). ^{13}C-NMR: δ 80.4 (C_1), 83.0 (C_2), 123.4, 123.6, 124.8 (C_5, C_{10}, C_{11}), 126.2 (C_3), 133.1 (C_4), 148.8 (C_{12}), 151.8 (C_6), 155.5 (C_9).

4.3. Syntheses of metal alkynyl complexes

4.3.1. *Trans-[Ru{(E)-4,4′-C≡CC$_6$H$_4$N=NC$_6$H$_4$NO$_2$}-Cl(dppm)$_2$] (**2**)*

Cis-[$RuCl_2$(dppm)$_2$] (90 mg, 0.096 mmol) (**1**) (30 mg, 0.12 mmol) and sodium hexafluorophosphate (40 mg, 0.24 mmol) were stirred in dichloromethane (10 ml) for 4 h at r.t. A solution of sodium methoxide (1 ml, 0.3 M solution in methanol) was added with stirring. The mixture was passed through a plug of alumina, eluting with dichloromethane, and the solvent was then removed on a rotary evaporator. The residue was recrystallized from dichloromethane–methanol to yield 75 mg (62%) of dark purple microcrystals identified as **2**. A crystal suitable for X-ray diffraction studies was grown by the slow diffusion of methanol into a dichloromethane solution. FABMS: 1155 ([M]$^+$, 40), 869 ([Ru(dppm)$_2$]$^+$, 20). Anal. Calc. for $C_{64}H_{52}ClN_3O_2P_4Ru$: C, 66.52; H, 4.54; N, 3.64. Found: C, 66.60; H, 4.24; N, 3.72%. UV–vis (λ_{max}, nm [ε, M^{-1} cm^{-1}]): 585 [27 200], 366 [14 000], 267 [41000]. IR (cm^{-1}): 2061 (w) ν(C≡C), 1341 (m) ν(N=O). ^{1}H-NMR: δ 4.93 (m, 4H, CH_2), 6.06 (d, 2H, $J_{HH} = 9$ Hz, H_4), 7.06–7.42 (m, 40H, Ph), 7.53 (d, 2H, $J_{HH} = 9$ Hz, H_5), 7.92 (d, 2H, $J_{HH} = 9$ Hz, H_{10}), 8.33 (d, 2H, $J_{HH} = 9$ Hz, H_{11}). ^{31}P-NMR: δ −6.3 (PPh_2). ^{13}C-NMR: δ 50.2 (CH_2), 117.5 (C_2), 122.7, 123.0, 124.7 (C_5, C_{10}, C_{11}), 127.6 (C_p), 129.2, 129.4 (C_m), 130.7 (C_4), 133.2, 133.4 (C_o), 134.3 (m, partially obscured by C_o, C_i) 136.0 (C_3), 147.6 (C_6), 148.0 (C_{12}), 156.6 (C_9).

4.3.2. *[Ru{(E)-4,4′-C≡CC$_6$H$_4$N=NC$_6$H$_4$NO$_2$}-(PPh$_3$)$_2$(η-C$_5$H$_5$)] (**3**)*

[$RuCl(PPh_3)_2(\eta\text{-}C_5H_5)$] (170 mg, 0.23 mmol) and **1** (70 mg, 0.28 mmol) were stirred in methanol (10 ml) at reflux for 30 min. The mixture was then cooled to r.t. and sodium methoxide solution (2 ml, 0.2 M solution in methanol) was added with stirring. The solvent was removed and the residue passed through a silica column eluting first with 3:5 dichloromethane–pet. spirit to remove excess alkyne, and then with 1:20 acetone–dichloromethane. The solvent was removed from the second fraction and the residue purified by thin-layer chromatography to yield 112 mg (51%) of dark purple microcrystals. FABMS: 941 ([M]$^+$, 55), 691 ([$Ru(PPh_3)_2(\eta\text{-}C_5H_5)$]$^+$, 40), 429 ([$Ru(PPh_3)(\eta\text{-}C_5H_5)$]$^+$, 70). Anal. Calc. for $C_{55}H_{43}N_3O_2P_2Ru$: C, 70.20; H, 4.61; N, 4.47. Found: C, 69.37; H, 4.60; N, 4.62%. UV–vis (λ_{max}, nm [ε, M^{-1} cm^{-1}]): 565 [28 600], 347 [17 300], 291 [16 800], 251 [24 500]. IR (cm^{-1}): 2054 (m) ν(C≡C), 1342 (m) ν(N=O). ^{1}H-NMR: δ 4.36 (s, 5H, C_5H_5), 7.07–7.47 (m, 32H, Ph), 7.80 (d, 2H, $J_{HH} = 8$ Hz, H_5), 7.96 (d, 2H, $J_{HH} = 9$ Hz, H_{10}), 8.34 (d, 2H, $J_{HH} = 9$ Hz, H_{11}). ^{31}P-NMR: δ 50.7 (PPh_3). ^{13}C-NMR: δ 85.6 (C_5H_5), 118.7 (C_2), 122.9, 123.8, 124.7 (C_5, C_{10}, C_{11}), 127.3 (t, $J_{CP} = 5$ Hz, C_m), 128.6 (C_p), 131.2 (C_4), 133.7 (t, $J_{CP} = 5$ Hz, CO), 135.7 (C_3), 138.5 (m, C_i), 147.7 (C_6), 148.5 (C_{12}), 156.5 (C_9).

4.3.3. *[Au{(E)-4,4′-C≡CC$_6$H$_4$N=NC$_6$H$_4$NO$_2$}(PPh$_3$)] (**4**)*

[$AuCl(PPh_3)$] (167 mg, 0.34 mmol), **1** (85 mg, 0.34 mmol) and sodium methoxide solution (1 ml, 0.5 M solution in methanol) were stirred in dichloromethane (5 ml) for 18 h. Methanol (10 ml) was then added and the volume reduced to ca. 10 ml whereupon the product precipitated. After filtration in air and washing with methanol (2×5 ml), 170 mg (71%) of orange–brown microcrystals were collected. FABMS: 721 ($[Au(PPh_3)_2]^+$, 15), 459 ($[Au(PPh_3)]^+$, 95). Anal. Calc. for $C_{32}H_{23}AuN_3O_2P$: C, 54.17; H, 3.27; N, 5.92. Found: C, 54.07; H, 3.18; N, 6.12%. UV–vis (λ_{max}, nm [ε, M^{-1} cm^{-1}]: 398 [32 800], 288 [14 000], 268 [17 400], 241 [32 000]. IR (cm^{-1}): 2113 (w) ν(C≡C), 1345 (s) ν_s(N=O). ^{1}H-NMR: δ 7.42–7.57 (m, 15H, Ph), 7.64 (d, 2H, $J_{HH} = 8$ Hz, H_4), 7.87 (d, 2H, $J_{HH} = 8$ Hz, H_5), 7.98 (d, 2H, $J_{HH} = 9$ Hz, H_{10}), 8.35 (d, 2H, $J_{HH} = 9$ Hz, H_{11}). ^{31}P-NMR: δ 42.6 (PPh_3). ^{13}C-NMR: δ 123.3, 124.7 (two of C_5, C_{10}, C_{11}), 129.2 (d, $J_{CP} = 6$ Hz, C_m), 131.6 (C_p), 133.2 (C_4), 134.2 (d, $J_{CP} = 14$ Hz, C_o), 148.4 (C_{12}), 150.6 (C_6), 155.8 (C_9).

4.4. X-ray structure determination

A purple needle ($0.40 \times 0.10 \times 0.05$ mm) grown by diffusion of methanol into a dichloromethane solution of **2** was mounted on a glass fiber. Data were collected on a Rigaku AFC6R diffractometer using graphite monochromated Cu–K_α radiation ($\lambda = 1.54178$ Å) at 296(1) K. The intensities of 9692 reflections were collected to $2\theta_{max} = 120.1°$; equivalent reflections were merged to yield 9120 unique reflections ($R_{int} = 0.049$). The intensities of three representative standards were measured after every 150 reflections to monitor stability and orientation. No decay correction was applied. An analytical absorption correction was applied which resulted in transmission factors ranging from 0.42 to 0.81. Data were corrected for Lorentz and polarization effects. The structure was solved by direct methods (SIR-92), and expanded using difference Fourier synthesis. The non-hydrogen atoms were refined with anisotropic displacement parameters, by minimizing $\Sigma w(|F_o| - |F_c|)^2$ where $w = [\sigma_c^2(F_o) + (p^2/4)F_o^2]^{-1}$. Hydrogen atoms were included in calculated positions but were not refined. The final cycle of full-matrix least-squares refinement was based on 5803 observed reflections ($I > 2\sigma(I)$) and 703 variable parameters. The maximum and minimum peaks in the final difference Fourier map corresponded to 0.98 and -0.89 e Å^{-3}, respectively. All calculations were performed using the TEXSAN [33] crystallographic software package.

Crystal data for $C_{64}H_{52}ClN_3O_2P_4Ru{\cdot}CH_2Cl_2$. $M_f = 1240.48$, monoclinic, space group, $P2_1/n$, $a = 10.242(4)$ Å, $b = 32.063(6)$ Å, $c = 18.310(4)$ Å, $\beta = 95.24(2)°$, $V = 5987(3)$ Å^3, $Z = 4$, $D_{calc} = 1.376$ g cm^{-3}, μ(Cu–K_α) = 47.30 cm^{-1}. $R = \Sigma(|F_o| - |F_c|)/\Sigma|F_o| = 0.053$, $R_w = [\{\Sigma w(|F_o| - |F_c|)^2\}/\Sigma wF_o^2]^{1/2} = 0.065$, GOF = 1.99.

4.5. Hyper-Rayleigh scattering measurements

An injection-seeded Nd:YAG laser (Q-switched Nd:YAG Quanta Ray GCR5, 1064 nm, 8 ns pulses, 10 Hz) was focussed into a cylindrical cell (7 ml) containing the sample. The intensity of the incident beam was varied by rotation of a half-wave plate placed between crossed polarizers. Part of the laser pulse was sampled by a photodiode to measure the vertically polarized incident light intensity. The frequency doubled light was collected by an efficient condenser system and detected by a photomultiplier. The harmonic scattering and linear scattering were distinguished by appropriate filters; gated integrators were used to obtain intensities of the incident and harmonic scattered light. The absence of a luminescence contribution to the harmonic signal was confirmed by using interference filters at different wavelengths near 532 nm. All measurements were performed in tetrahydrofuran using *p*-nitroaniline ($\beta = 21.4 \times 10^{-30}$ esu) [34] as a reference. Solutions were sufficiently dilute that absorption of scattered light was negligible. Further details of the experimental procedure have been reported in the literature [35,36].

5. Supplementary material

Crystallographic data for the structure reported in the paper have been deposited with the Cambridge Crystallographic Data Centre, CCDC No. 139410 for compound **2**. Copies of this information may be obtained free of charge from The Director, CCDC, 12 Union Road, Cambridge, CB2 1EZ, UK (fax: +44-1223-336033; e-mail: deposit@ccdc.cam.ac.uk or www: http://www.ccdc.cam.ac.uk).

Acknowledgements

We thank the Fund for Scientific Research-Flanders (G.0338.98, G.0407.98) (A.P.), the Belgian Government (IUAP-IV/11) (AP), the K.U. Leuven (GOA/2000/03) (A.P.), and the Australian Research Council (M.G.H.) for financial support, and Johnson Matthey Technology Centre for the loan of ruthenium salts (M.G.H.). S.H. is a postdoctoral researcher of the Fund for Scientific Research-Flanders, M.G.H. is an ARC Australian Senior Research Fellow, A.M.M. held and N.T.L. holds an Australian Postgraduate Award.

References

[1] H.S. Nalwa, in: H.S. Nalwa, S. Miyata (Eds.), Nonlinear Optics of Organic Molecules and Polymers, CRC, Boca Raton, 1997.

[2] D.S. Chemla, J. Zyss (Eds.), Nonlinear Optical Properties of Organic Molecules and Crystals, vol. I, Academic, Orlando, 1987.

[3] D.S. Chemla, J. Zyss (Eds.), Nonlinear Optical Properties of Organic Molecules and Crystals, vol. II, Academic, Orlando, 1987.

[4] R.A. Hann, D. Bloor (Eds.), Organic Materials for Nonlinear Optics, Royal Society of Chemistry, London, 1989.

[5] R.A. Hann, D. Bloor (Eds.), Organic Materials for Nonlinear Optics II, Royal Society of Chemistry, London, 1991.

[6] G.J. Ashwell, D. Bloor (Eds.), Organic Materials for Nonlinear Optics III, Royal Society of Chemistry, Cambridge, 1993.

[7] J.H. Williams, Acc. Chem. Res. 26 (1993) 593.

[8] K.D. Singer, J.E. Sohn, L.A. King, H.M. Gordon, H.E. Katz, C.W. Dirk, J. Opt. Soc. Am. B 6 (1989) 1339.

[9] C.A. van Walree, O. Franssen, A.W. Marsman, M.C. Flipse, L.W. Jennekens, J. Chem. Soc. Perkin Trans. 2 (1997) 799.

[10] A. Hilton, T. Renouard, O. Maury, H. Le Bozec, I. Ledoux, J. Zyss, J. Chem. Soc. Chem. Commun. (1999) 2521.

[11] S.R. Marder, L.E. Sohn, G.D. Stucky (Eds.), Materials for Nonlinear Optics, Chemical Perspectives, American Chemical Society, Washington DC, 1991.

[12] N.J. Long, Angew. Chem. Int. Ed. Engl. 34 (1995) 21.

[13] T. Verbiest, S. Houbrechts, M. Kauranen, K. Clays, A. Persoons, J. Mater. Chem. 7 (1997) 2175.

[14] I.R. Whittall, A.M. McDonagh, M.G. Humphrey, M. Samoc, Adv. Organomet. Chem. 43 (1999) 349.

[15] I.R. Whittall, A.M. McDonagh, M.G. Humphrey, M. Samoc, Adv. Organomet. Chem. 42 (1998) 291.

[16] I.R. Whittall, M.G. Humphrey, A. Persoons, S. Houbrechts, Organometallics 15 (1996) 1935.

[17] I.R. Whittall, M.G. Humphrey, S. Houbrechts, A. Persoons, D.C.R. Hockless, Organometallics 15 (1996) 5738.

[18] I.R. Whittall, M.P. Cifuentes, M.G. Humphrey, B. Luther-Davies, M. Samoc, S. Houbrechts, A. Persoons, G.A. Heath, D.C.R. Hockless, J. Organomet. Chem. 549 (1997) 127.

[19] I.R. Whittall, M.P. Cifuentes, M.G. Humphrey, B. Luther-Davies, M. Samoc, S. Houbrechts, A. Persoons, G.A. Heath, D. Bogsanyi, Organometallics 16 (1997) 2631.

[20] R.H. Naulty, M.P. Cifuentes, M.G. Humphrey, S. Houbrechts, C. Boutton, A. Persoons, G.A. Heath, D.C.R. Hockless, B. Luther-Davies, M. Samoc, J. Chem. Soc. Dalton Trans. (1997) 4167.

[21] I.R. Whittall, M.G. Humphrey, S. Houbrechts, J. Maes, A. Persoons, S. Schmid, D.C.R. Hockless, J. Organomet. Chem 544 (1997) 277.

[22] R.H. Naulty, A.M. McDonagh, I.R. Whittall, M.P. Cifuentes, M.G. Humphrey, S. Houbrechts, J. Maes, A. Persoons, G.A. Heath, D.C.R. Hockless, J. Organomet. Chem. 563 (1998) 137.

[23] A. Vogel, Textbook of Practical Organic Chemistry, Longman, London, 1978.

[24] S. Takahashi, Y. Kuroyama, K. Sonogashira and N. Hagihara, Synthesis (1980) 627.

[25] D. Touchard, P. Haquette, N. Pirio, L. Toupet, P.H. Dixneuf, Organometallics 12 (1993) 3132.

[26] M.I. Bruce, R.C. Wallis, Aust. J. Chem. 32 (1979) 1471.

[27] A.M. McDonagh, I.R. Whittall, M.G. Humphrey, B.W. Skelton, A.H. White, J. Organomet. Chem. 519 (1996) 229.

[28] I.R. Whittall, M.G. Humphrey, D.C.R. Hockless, B.W. Skelton, A.H. White, Organometallics 14 (1995) 3970.

[29] S. Houbrechts, K. Clays, A. Persoons, V. Cadierno, M.P. Gamasa, J. Gimeno, I.R. Whittall, M.G. Humphrey, Proc. SPIE — Int. Soc. Opt. Eng. 2852 (1996) 98.

[30] S. Houbrechts, C. Boutton, K. Clays, A. Persoons, I.R. Whittall, R.H. Naulty, M.P. Cifuentes, M.G. Humphrey, Int. J. Nonlinear Opt. Phys. 7 (1998) 113.

[31] M.I. Bruce, C. Hamiester, A.G. Swincer, R.C. Wallis, Inorg. Synth. 21 (1982) 78.

[32] M.I. Bruce, B.K. Nicholson, O. Bin Shawkataly, Inorg. Synth. 26 (1989) 324.

[33] TEXSAN, Single Crystal Structure Analysis Software, Version 1.7-3, Molecular Structure Corporation, The Woodlands, TX, USA, 1995.

[34] M. Stahelin, D.M. Burland, J.E. Rice, Chem. Phys. Lett. 191 (1992) 245.

[35] K. Clays, A. Persoons, Rev. Sci. Instrum. 63 (1992) 3285.

[36] S. Houbrechts, K. Clays, A. Persoons, Z. Pikramenou, J.M. Lehn, Chem. Phys. Lett. 258 (1996) 485.

[37] A.J. Hodge, S.L. Ingham, A.K. Kakkar, M.S. Khan, J. Lewis, N.J. Long, D.G. Parker, P.R. Raithby, J. Organomet. Chem. 488 (1995) 205.

[38] B. Chaudret, G. Commenges, R. Poiblanc, J. Chem. Soc. Dalton Trans. (1984) 1635.